Roger Zebaze   ORCID iD: 0000-0001-7406-9658

Marit Osima   ORCID iD: 0000-0002-7114-7857

Xiao-Fang Wang   ORCID iD: 0000-0003-3246-3205

Peter Ebeling   ORCID iD: 0000-0002-2921-3742

Ego Seeman   ORCID iD: 0000-0002-9692-048X

Åshild Bjørnerem   ORCID iD: 0000-0002-3123-2950

Adding Marrow Adiposity and Cortical Porosity to Femoral Neck Areal Bone Mineral Density Improves the Discrimination of Women with Nonvertebral Fractures from Controls

Running head: Marrow adiposity, cortical porosity and fracture

Roger Zebaze,[1,2]* Marit Osima,[3,4]* Minh Bui,[5] Marko Lukic,[3] Xiaofang Wang,[2] Ali Ghasem-Zadeh,[2] Erik F Eriksen,[6,7] Angela Vais[8], Catherine Shore-Lorenti,[1] Peter Ebeling[1], Ego Seeman,[2,9] Åshild Bjørnerem[10,11]

[1]Department of Medicine, School of Clinical Sciences, Monash Health, Monash University, Melbourne, Australia

[2]Departments of Medicine and Endocrinology, Austin Health, University of Melbourne, Melbourne, Australia

[3]Department of Community Medicine, UiT The Arctic University of Norway, Tromsø, Norway

[4]Department of Orthopaedic Surgery, University Hospital of North Norway, Tromsø, Norway

[5]Centre for Epidemiology and Biostatistics, School of Population and Global Health, University of Melbourne, Melbourne, Australia

[6]Department of Endocrinology, Morbid Obesity and Preventive Medicine, Oslo University Hospital, Oslo, Norway

[7]Department of Clinical Medicine, University of Oslo, Oslo, Norway

[8]Hudson Institute for Medical Research, Monash University, Melbourne, Australia

[9]Mary MacKillop Institute for Health Research, Australian Catholic University, Melbourne, Australia

[10]Department of Clinical Medicine, UiT The Arctic University of Norway, Tromsø, Norway

[11]Depatment of Obstetrics and Gynecology, University Hospital of North Norway, Tromsø, Norway

Corresponding author: Roger Zebaze, MD

Department of Medicine, School of Clinical Sciences, Monash Health,   Monash University, 246 Clayton Rd, Clayton, VIC 3168, Australia
Email:Roger.Zebaze@monash.edu

*These two authors contributed equally to this manuscript

ABSTRACT

Advancing age is accompanied by a reduction in bone formation and remodeling imbalance, which produces microstructural deterioration. This may be partly due to diversion of mesenchymal cells towards adipocytes rather than osteoblast lineage cells. We hypothesized that microstructural deterioration will be associated with an increased marrow adiposity, and each of these traits will be independently associated with nonvertebral fractures and improve discrimination of women with fractures from controls over that achieved by femoral neck (FN) areal bone mineral density (aBMD) alone. The marrow adiposity and bone microstructure were quantified from high-resolution peripheral quantitative computed tomography (HR-pQCT) images of the distal tibia and distal radius in 77 women aged 40-70 years with a recent nonvertebral fracture and 226 controls in Melbourne, Australia. Marrow fat measurement from HR-

pQCT images was validated using direct histologic measurement as gold standard, at the distal radius of 15 sheep, with an agreement ($R^2 = 0.86$, $p < 0.0001$). Each standard deviation (SD) higher distal tibia marrow adiposity was associated with 0.33 SD higher cortical porosity, 0.60 SD fewer, 0.24 SD thinner and 0.72 SD more separated trabeculae (all $p < 0.05$). Adjusted for age and FN aBMD, odds ratios (95% confidence interval) for fracture per SD higher marrow adiposity and cortical porosity were 3.39 (2.14-5.38) and 1.79 (1.14-2.80), respectively. Discrimination of women with fracture from controls improved when cortical porosity was added to FN aBMD and age (AUC 0.778 vs. 0.751, $p = 0.006$) or marrow adiposity was added to FN aBMD and age (AUC 0.825 vs. 0.751, $p = 0.002$). The model including FN aBMD, age, cortical porosity, trabecular thickness and marrow adiposity had an AUC = 0.888. Results were similar for the distal radius. Whether marrow adiposity and cortical porosity indices improve identification of women at risk for fractures requires validation in prospective studies.

Key Words Cortical porosity, HR-pQCT, marrow adiposity, nonvertebral fracture, women

Introduction

Ageing is associated with development of abnormalities in bone remodeling.[1] Around midlife in women, remodeling becomes unbalanced and rapid. Less bone is deposited than resorbed by each remodeling event resulting in microstructural deterioration. Porosity increases, cortices thin and become fragmented, trabeculae thin, perforate and may eventually disappear.[2-5] Unbalanced remodeling upon the endocortical surface erodes the cortex and increases the medullary compartment volume, which in turn becomes occupied by fat cells, non-fat cells and extracellular water.

The mechanisms responsible for the reduction in the volume of bone deposited by each remodeling event are unclear. However, osteoblasts and adipocytes share common precursor cells in the bone marrow, and decreased bone formation may be partly the result of enhanced adipogenesis in favour of osteoblastogenesis.[6-10]

There is an age-related increase in marrow adiposity and a reciprocal reduction in trabecular bone volume.[11-14] We propose that the proportions of this non-mineral compartment can be distinguished because fat cells attenuate photons less than the attenuation produced by water and non-fat cells.[15,16] Accordingly, we validated a method for identifying marrow adipose tissue from high-resolution peripheral quantitative computed tomography (HR-pQCT) images and we estimated a marrow adiposity index.

Combining microstructural deterioration with areal bone mineral density (aBMD) and the Fracture Risk Assessment Tool (FRAX) leaves more than half of the women with fractures unidentified.[17] We hypothesized that a higher marrow adiposity index, will be associated with microstructural deterioration and contribute to fracture risk independently of cortical porosity, and each will improve discrimination of women with fractures from controls when added to femoral neck aBMD.

Materials and Methods

Validation of marrow fat assessment using HR-pQCT with histology as gold standard

It has been shown using histologic assessment as gold standard, that Dual Energy Computed Tomography (DECT) can be used to accurately measure marrow fat.[18] We determined whether marrow fat could be accurately measured from images acquired

using HR-pQCT and analyzed using StrAx software, with co-registered histologic examinations as gold standard. Twenty fresh sheep radii specimens were collected and stored at -20 degrees Celsius. Sheep are commonly used as animal model for research in bone diseases, because their bone architecture is similar to that of humans.[19] Specimens were sectioned at a 1.5 cm location proximal to the sheep wrist joint. The proximal part was sealed to avoid any loss of fat or bone tissue and scanned using HR-pQCT. After HR-pQCT imaging, proximal parts were cut and a 1 cm thick sections was kept. These sections were decalcified. The sections were cut into left and right halves to fit the field of view of the microscope for histological imaging. Each half was embedded in paraffin wax and stained with hematoxylin and eosin (H&E). The scanning protocol ensured that the first HR-pQCT slice corresponded to the histological section in which marrow fat was measured. The process of co-registration of histologic cross-sections with HR-pQCT imaging; and an example of adipose tissue seen after H&E staining is shown in Fig. 1.

HR-pQCT imaging and marrow fat measurement

A 110 HR-pQCT slices were obtained from the distal end of sheep radii and scanned moving proximally as per manufacturer protocol used to collect HR-pQCT images *in vivo* with an Xtreme CT II (Scanco Medical AG, Brüttisellen, Switzerland) but using XtremeCT I equivalent protocol. Images were analysed using StrAx software. The proportion of fat voxels within the marrow cavity – i.e. adipose volume (AV) to total marrow volume (TV) was outputted.

Histological imaging and marrow fat measurement

A full digital image of each half cross-section was captured using Olympus VS120 microscope (Olympus Corporation manufacturer, Tokyo. Japan) with a color camera

at X 20 magnification. The images were analyzed using ImageJ.[20] In brief, the scale was calibrated to 512 pixels/mm and the images were converted to an 8-bit gray scale. The trabecular compartment in each cross-sectional half was segmented. Areas in the marrow cavity occupied by adipocyte tissue were identified as void spaces remaining from the H&E staining. Areas with artifacts were avoided during the quantification process. AV/TV was calculated for each half. After excluding 5 of the 20 samples with artifacts such as folding during preparation, the analysis was restricted to the remaining 15 samples.

Subjects

We recruited 84 women above 40 years of age within 14 days of having had a nonvertebral fracture, to minimize the likelihood that changes in cortical porosity or medullary composition was following the fracture (Fig. 2). These women presented to the Emergency Department at Austin Health, Melbourne, Australia. The 84 fracture cases had fracture at the distal forearm (n = 52), upper arm (n = 5), elbow (n = 5), hand (n = 2), rib (n = 1), hip (n = 3), lower leg (n = 6), ankle (n = 9), and toe (n = 1). After excluding 5 women receiving hormone replacement therapy (HRT), and 2 and 10 women with movement artifact during image acquisition of distal tibia and distal radius, 77 and 69 women with fracture remained with valid measurements of distal tibia and distal radius, respectively.

We compared the measurements with those of healthy twins from the Twins Research Australia (n = 653).[3,21,22] Among these controls, we excluded 30 women taking HRT, 108 women below 40 years of age and 170 women with a prior fracture, 11 and 37 women with movement artifacts of distal tibia and distal radius, leaving 334 and 308 controls with valid measurements of distal tibia and distal radius,

respectively. Of the 334 controls with valid measurements of distal tibia, 118 were singletons and 216 were twins. We randomly selected one twin from each pair (n = 108), and 118 + 108 = 226 singletons were left included as controls in the analysis of distal tibia measurements. Of the 308 controls with valid measurements of distal radius, 120 were singletons and 188 were twins. We randomly selected one twin for each pair (n = 94), and 120 + 94 = 214 singletons were left included as controls in the analysis of distal radius measurements.

The participants answered a questionnaire including information on their prior fracture, diseases, use of medication, menstruation, menopause and lifestyle, including weekly hours they participated in light (walking, lawn bowls, light gardening), moderate (social tennis, golf, hiking) or vigorous physical activity (competitive active sports). A physical activity index was made by adding hours of light, moderate and vigorous activity, giving the hours with moderate and vigorous physical activity double and triple weight: index = light + 2moderate + 3vigorous. Women were classified as postmenopausal (amenorrhea for more than 1 year), perimenopausal (no cycles for 3-12 months) and premenopausal (a regular cycle in the last 3 months). All women gave written informed consent. The Austin Health Human Research Ethics Committee approved the study.

Measurements

Height and weight were measured while wearing light clothing and no shoes. HR-pQCT (XtremeCT, Scanco Medical AG, Brüttisellen, Switzerland, isotropic resolution of 82 μm) was used to obtain images at the nondominant distal tibia and distal radius.[23] In those with fracture at the nondominant side, the opposite side was scanned. The 110 CT slices were obtained at a standardized distance of 22.5 and 9.5

mm from a reference line that was manually placed at the endplate of the distal tibia and distal radius, respectively. The 49 most proximal slices in 110 slices of region of interest were chosen because the thicker cortex allows accurate assessment of cortical porosity.[21,22,24]

Cortical and trabecular morphology and a marrow adiposity index, a surrogate marrow fat, were quantified using StrAx software (StraxCorp, Melbourne, Australia), a non-threshold based method that selects attenuation profile curves and segments the bone into the compact-appearing cortex, outer (OTZ) and inner transitional zones (ITZ), and trabecular compartment.[25] Local bone edges were identified as the beginning and the end of the rising and falling S-shaped portions of the profile curve enabling the delineation of the compartments. The density profile curve produced had two plateaus; one corresponding to the compact-appearing cortex and one corresponding to the trabecular compartment. Between these plateaus was a descending S-shaped curve or transition between the two plateaus. This was the transitional zone.[25] The porosity quantified by the StrAx algorithm is the proportion of void within each voxel. This method confine cortical porosity and cortical fragments to the transitional zone, and not to the medullary canal yielding a higher cortical porosity than reported using threshold based methods.[25,26] The precision of the measurements had coefficients of variation (CV) < 4%.[25] Trabecular number, thickness, separation, trabecular bone volume per tissue volume (BV/TV) and volumetric BMD (vBMD) were also quantified using the StrAx software.

The medullary canal contains fat cells, mineralized matrix, non-fat cells and water. Voxels containing fat cells can be identified because their photons attenuation is below that of water. Thus, in HR-pQCT images, adipose volume (AV) was defined

as the total volume of the marrow cavity (TV) occupied by voxels with attenuation below that of water. We expressed the fat proportion (FP) = 100 * AV/TV (%). As age-related endocortical resorption increases the medullary cavity, this reduces the fat proportion but not the nonmineral apparent density produced by the fat cells, non-fat cells and water. We calculated a relative medullary density (RMD) as a percentage of fully mineralized bone matrix (1200 mg HA/cm³). As the RMD decreases as fat cells increase, we subtracted this value from 100 for ease of comprehension, and RMD $(\%) = 100 - [100 * \frac{\text{Mean Medullary Density}}{1200}]$ (Fig. 3). The Marrow Adiposity Index (MAI) is a function of the fat proportion and the relative medullary density, MAI = $\frac{FP*RMD}{100}$. As we did not measure the absolute content of fat cells in the medullary cavity, we refer to a medullary adiposity index as an indicator of the presence of fat cells.

Femoral neck (FN) aBMD was assessed using dual-energy x-ray absorptiometry (DXA, Lunar Prodigy, Lunar Corporation, Madison, WI, USA) at the left femur, and CV was 2.6%. The women were categorized into those with normal FN aBMD (T score > -1.0), osteopenia (T-score between -2.5 and -1.0) and osteoporosis (T-score < -2.5) using the World Health Organization (WHO) classification.[27]

Statistical analyses

To validate StrAx software quantification of marrow fat in sheep radii, linear regression was used to determine the R^2 between the gold-standard and StrAx measurements. The Root Mean Square Error (RMSE) between StrAx measurement and the gold standard was quantified. Bland-Altman Plot was used to assess the difference between the two measurement methods.

In women, summary statistics are presented as mean and standard deviation (SD). We compared distal tibia and distal radius parameters in cases and controls, taking into account the menopausal status, physical activity and age, using a semi-parametric regression model. We used fracture status, menopausal status, and physical activity as parametric variables and age as a non-parametric variable, because age had a non-linear relationship with bone parameters, with almost no change from 40 until about 47 years of age. Menopausal status alone was associated with bone parameters before but not after adjustment for age. The semi-parametric regression models were also used to assess the associations of cortical and trabecular morphology as a function of the marrow adiposity index, adjusted for height, weight, physical activity and fracture status (when significant) as parametric variables, and age as a non-parametric variable. Coefficients and standard errors (SE) with three decimals, exact p-values and R-square are presented together to illustrate which of the variables are most strongly associated.

Odds ratio (OR) for fracture per 1 SD change in cortical porosity, marrow adiposity index and other cortical and trabecular bone morphology were calculated in logistic regression analyses adjusted for age (quadratic model) and FN aBMD. Distal tibia and distal radius variables were standardised to have mean = 0 and SD = 1 in the linear and logistic regression analysis. In final multivariable models, we combined cortical porosity and marrow adiposity index in the same models, adjusted for age, FN aBMD and covariates that were the best subsets of variables.[28] We calculated area under the receiver operating characteristic curve (AUC) using logistic regression analysis to determine whether discrimination of women with fractures from controls was improved when adding microstructure and marrow adiposity index to the reference model 1 (age, age² and FN aBMD), and the reference model 2 (age, age²,

FN aBMD and marrow adiposity index). The final models were also adjusted for significant covariates. Chi-square p-value was used to compare the AUC after additional adjustment for covariates. Analyses were performed using STATA Software package, v14 (StataCorp, LP, Texas, USA) and SAS software package, v9.4 (SAS Institute Inc., Cary, NC, USA). All tests were two-sided and $p < 0.05$ considered significant.

Results

Accuracy of the marrow fat measurement in sheep radii

AV/TV measured from HR-pQCT images using StrAx predicted the gold standard histological measurement of marrow with an R^2 of 0.86 ($p < 0.001$) and a RMSE of 0.96% (Fig. 4). Bland-Altman Plot showed that HR-pQCT overestimated AV/TV by on average 2.67 ± 1.00 % ($p < 0.001$).

Marrow adiposity index is associated with microstructure

Fracture cases had higher distal tibial marrow adiposity index, higher porosity, lower trabecular BV/TV and FN aBMD than controls, adjusted for menopausal status, physical activity and age (all $p < 0.01$, Table 1). Each SD higher medullary adiposity index was associated with 0.14, 0.17 and 0.80 SD higher porosity of the compact appearing cortex, outer and inner transitional zones, 0.16 SD thinner cortices, 0.60 SD lower trabecular number, 0.24 SD thinner and 0.72 SD more separated trabeculae (all $p \leq 0.01$, Table 2). Marrow adiposity index explained 5 to 66% of the variance in cortical and 10 to 86% of the variance in trabecular parameters. All results were adjusted for age, fracture status, physical activity, height and weight. Results were similar for distal radius as shown in Table 1 and Table 2.

Marrow adiposity index and cortical porosity improved discrimination of fractures

Each SD increment in marrow adiposity index of distal tibia was associated with fractures adjusted for age, FN aBMD and cortical porosity (OR 3.39, 95% confidence interval (CI) 2.14-5.38, Table 3). Each SD higher cortical porosity was associated with fractures adjusted for age, FN aBMD and marrow adiposity index (OR 1.79, 95% CI 1.14-2.80). There were no interactions between marrow adiposity index, FN aBMD or cortical porosity. Discrimination of women with fractures from controls was improved when distal tibia cortical porosity was added to FN aBMD and age (AUC 0.778 vs. 0.751, p = 0.006) or marrow adiposity index was added to FN aBMD and age (AUC 0.825 vs. 0.751, p = 0.002) (Table 4). The model including distal tibia cortical porosity, trabecular thickness, marrow adiposity index, FN aBMD, age and weight had an AUC = 0.888. Results were similar for distal radius as shown in Table 3 and Table 4.

Discussion

We report that marrow fat can be accurately measured from the analysis of HR-pQCT images acquired *in vivo* in clinical and research settings. We further extended these findings by showing that marrow fat so measured can be used to produce a marrow adiposity index that improves the identification of women with nonvertebral fractures and does so independently of other metrics such as cortical porosity and FN aBMD.

Historically, clinical assessment of marrow adiposity required a bone biopsy. Recently, with advancing in imaging techniques, there is increasing evidence that the role of marrow adiposity on skeletal health can be studied directly and non-invasively.

Until lately, non-invasive assessment of marrow fat has been limited to Magnetic Resonance Imaging (MRI). However, MRI is not readily available for the purpose of quantifying marrow fat, and is costly. Thus, the need to develop more readily available, inexpensive and rapid approaches to quantify bone marrow fat in *in vivo* settings. It is reported that marrow fat measured from histological images processed after H&E staining agreed with marrow fat quantified using *in vivo* imaging modalities-i.e., DECT and MRI.[25] There are also studies showing that single energy high resolution-QCT can be used to measured marrow fat.[29] In this study, we complemented these findings, by showing that marrow fat measured from HR-pQCT images showed an excellent correlation with marrow fat measured from histological images after H&E staining.

Most fragility fractures occur in women with osteopenia or normal aBMD, not women with osteoporosis.[30] High vertebral marrow adiposity is associated with vertebral fracture independent of aBMD,[13,31] Vertebral marrow adiposity is 10% and 5% higher in patients with osteoporosis and osteopenia without fracture, respectively, compared to age-matched healthy controls,[15,31-34] suggesting an association between marrow adiposity and aBMD.[15] We found that the distal tibia marrow adiposity index, together with cortical porosity and trabecular thickness best discriminated women with fracture from controls, and did so independent of FN aBMD and age. Another study reported that a combination of cortical and trabecular microstructure improved fracture prediction.[35]

Marrow adiposity was associated with porosity of each cortical compartments, particularly of the inner transitional zone adjacent to the medullary cavity. However, the association between marrow adiposity index and the porosity of the compact

cortex, located more distant from the marrow cavity, is likely to be more important in compromising bending strength.[36] Marrow adiposity index was also associated with fewer, thinner more separated trabeculae, lower trabecular BV/TV and vBMD. Nevertheless, marrow adiposity index was associated with fracture prevalence independently of cortical and trabecular microstructure. We also took into account height, weight, physical activity and the menopausal status in the analysis of this current study, however, when the effect of age was taken into account, the menopausal status made no additional contribution to the association between bone and fat traits.

The reasons for the association of marrow adiposity index with deteriorated microstructure and the improved discrimination of fractures independently of bone microstructure are unclear. There may be a shift from osteogenesis to adipogenesis, remodeling imbalance, leading to reduced bone strength, and thus increase in fracture risk.[10,37]

Low estrogen levels after menopause may contribute to increased adipogenesis, as estrogen treatment of osteoporotic postmenopausal women prevented increase in marrow adiposity compared with controls treated with placebo.[10,38] In the only study that we are aware of using pQCT for quantification of marrow cavity fat, loading was associated with lower marrow fat, which in turn was associated with greater bone strength, larger midtibial cortical area, not cortical vBMD.[39] In a study using MRI, runners had lower lumbar vertebral marrow fat fraction than non-sporting controls, suggesting that exercise may reduce the age-related increase in marrow adiposity.[40]

This study has several limitations. As it was cross-sectional, we could not assess causation between marrow adiposity, microstructure and fracture. From HR-

pQCT images, we assessed voxels within the marrow cavity not occupied by bone. The other components of those voxels are fat cells, non-fat content such as other cells and water. As we did not measure the absolute content of fat cells in the marrow cavity, we refer to a marrow adiposity index, an indicator of the presence of fat cells. Nevertheless, marrow fat measured from HR-pQCT images and directly from histological images showed agreement. As compared to histologic measurements, HR-pQCT overestimated marrow fat with a bias by on average 2.67%. This bias can be explained by a partial volume effect resulting from voxels containing marrow fat and mineralized bone matrix at the edge between trabeculae and marrow fat are classified as fat voxels in HR-pQCT images. Increased marrow adiposity can result in considerable measurement errors in aBMD,[41,42] and may have confounded the associations observed in the current study to some unknown extent.

In summary, marrow fat can be accurately measured from HR-pQCT images and used *in vivo* to provide a marrow adiposity index. A higher marrow adiposity index was associated with microstructural deterioration and the presence of nonvertebral fractures independent of this microstructural deterioration and femoral neck aBMD. Discrimination of fracture cases from controls may be improved when marrow adiposity and cortical porosity are combined with femoral neck aBMD. Prospective studies are needed to validate these observations.

Disclosures

is a director of the board and shareholder in StraxCorp. Eriksen is a member of the advisory board for Amgen, MSD, Novartis and Lilly and has received consulting fees from IDS, and speaker fees from Amgen, MSD, Novartis and Lilly. All authors state that they have no other conflicts of interest.

References

1. Seeman E, Delmas PD. Bone quality—the material and structural basis of bone strength and fragility. N Engl J Med. 2006;354(21):2250-61.

2. Seeman E. Age-and menopause-related bone loss compromise cortical and trabecular microstructure. J Gerontol A Biol Sci Med Sci. 2013;68(10):1218-25.

3. Bjørnerem Å, Ghasem-Zadeh A, Bui M, Wang X, Rantzau C, Nguyen TV, et al. Remodeling markers are associated with larger intracortical surface area but smaller trabecular surface area: a twin study. Bone. 2011;49(6):1125-30.

4. Shigdel R, Osima M, Ahmed LA, Joakimsen RM, Eriksen EF, Zebaze R, et al. Bone turnover markers are associated with higher cortical porosity, thinner cortices, and larger size of the proximal femur and non-vertebral fractures. Bone. 2015;81:1-6.

5. Shigdel R, Osima M, Lukic M, Ahmed LA, Joakimsen RM, Eriksen EF, et al. Determinants of Transitional Zone Area and Porosity of the Proximal Femur Quantified In Vivo in Postmenopausal Women. J Bone Miner Res. 2016;31(4)758-66.

6. Moerman EJ, Teng K, Lipschitz DA, Lecka-Czernik B. Aging activates adipogenic and suppresses osteogenic programs in mesenchymal marrow stroma/stem cells: the role of PPAR-γ2 transcription factor and TGF-βBMP signaling pathways. Aging Cell. 2004;3(6):379-89.

7. Abdallah BM, Haack-Sørensen M, Fink T, Kassem M. Inhibition of osteoblast differentiation but not adipocyte differentiation of mesenchymal stem cells by sera obtained from aged females. Bone. 2006;39(1):181-8.

8. Song L, Liu M, Ono N, Bringhurst FR, Kronenberg HM, Guo J. Loss of wnt/β-catenin signaling causes cell fate shift of preosteoblasts from osteoblasts to adipocytes. J Bone Miner Res. 2012;27(11):2344-58.

9.   Muruganandan S, Roman A, Sinal C. Adipocyte differentiation of bone marrow-derived mesenchymal stem cells: cross talk with the osteoblastogenic program. Cell Mol Life Sci. 2009;66(2):236-53.

10.   Fazeli PK, Horowitz MC, MacDougald OA, Scheller EL, Rodeheffer MS, Rosen CJ, et al. Marrow fat and bone—new perspectives. J Clin Endocrinol Metab. 2013;98(3):935-45.

11.   Rosen CJ, Bouxsein ML. Mechanisms of disease: is osteoporosis the obesity of bone? Nat Clin Pract Rheumatol. 2006;2(1):35-43.

12.   Justesen J, Stenderup K, Ebbesen E, Mosekilde L, Steiniche T, Kassem M. Adipocyte tissue volume in bone marrow is increased with aging and in patients with osteoporosis. Biogerontology. 2001;2(3):165-71.

13.   Schwartz AV, Sigurdsson S, Hue TF, Lang TF, Harris TB, Rosen CJ, et al. Vertebral bone marrow fat associated with lower trabecular BMD and prevalent vertebral fracture in older adults. J Clin Endocrinol Metab. 2013;98(6):2294-300.

14.   Devlin MJ, Rosen CJ. The bone–fat interface: basic and clinical implications of marrow adiposity. Lancet Diabetes Endocrinol. 2015;3(2):141-7.

15.   Veldhuis-Vlug AG, Rosen CJ. Mechanisms of marrow adiposity and its implications for skeletal health. Metabolism. 2017;67:106-14.

16.   Vogler 3rd J, Murphy W. Bone marrow imaging. Radiology. 1988;168(3):679-93.

17. Ahmed LA, Shigdel R, Joakimsen R, Eldevik O, Eriksen E, Ghasem-Zadeh A, et al. Measurement of cortical porosity of the proximal femur improves identification of women with nonvertebral fragility fractures. Osteoporos Int. 2015;26(8):2137-46.

18. Arentsen L, Yagi M, Takahashi Y, Bolan PJ, White M, Yee D, Hui S. Validation of marrow fat assessment using noninvasive imaging with histologic examination of human bone samples. Bone. 2015;72:118-22.

19. Turner AS. The sheep as a model for osteoporosis in humans. Vet J. 2002;163(3):232-9.

20. Schindelin J, Arganda-Carreras I, Frise E, Kaynig V, Longair M, Pietzsch T, et al. Fiji: an open-source platform for biological-image analysis. Nat Methods 2012;9(7):676-82.

21. Bjørnerem Å, Bui QM, Ghasem-Zadeh A, Hopper JL, Zebaze R, Seeman E. Fracture risk and height: an association partly accounted for by cortical porosity of relatively thinner cortices. J Bone Miner Res. 2013;28(9):2017-26.

22. Bjørnerem Å, Bui M, Wang X, Ghasem-Zadeh A, Hopper JL, Zebaze R, et al. Genetic and environmental variances of bone microarchitecture and bone remodeling markers: a twin study. J Bone Miner Res. 2015;30(3):519-27.

23. Laib A, Häuselmann HJ, Rüegsegger P. In vivo high resolution 3D-QCT of the human forearm. Technol Health Care. 1998;6(5-6):329-37.

24. Bala Y, Zebaze R, Ghasem-Zadeh A, Atkinson EJ, Iuliano S, Peterson JM, et al. Cortical porosity identifies women with osteopenia at increased risk for forearm fractures. J Bone Miner Res. 2014;29(6):1356-62.

25. Zebaze R, Ghasem-Zadeh A, Mbala A, Seeman E. A new method of segmentation of compact-appearing, transitional and trabecular compartments and quantification of cortical porosity from high resolution peripheral quantitative computed tomographic images. Bone. 2013;54(1):8-20.

26. Zebaze RM, Ghasem-Zadeh A, Bohte A, Iuliano-Burns S, Mirams M, Price RI, et al. Intracortical remodelling and porosity in the distal radius and post-mortem femurs of women: a cross-sectional study. Lancet. 2010;375(9727):1729-36.

27. Looker AC, Orwoll ES, Johnston CC, Lindsay RL, Wahner HW, Dunn WL, et al. Prevalence of low femoral bone density in older US adults from NHANES III. J Bone Miner Res. 1997;12(11):1761-8.

28. Lawless J, Singhal K. Efficient screening of nonnormal regression models. Biometrics. 1978:318-27.

29. Peña JA, Thomsen F, Damm T, Campbell GM, Bastgen J, Barkmann R, Glüer CC. Bone-marrow densitometry: Assessment of marrow space of human vertebrae by single energy high resolution-quantitative computed tomography. Med Phys. 2016;43(7):4174.

30. Siris ES, Chen Y-T, Abbott TA, Barrett-Connor E, Miller PD, Wehren LE, et al. Bone mineral density thresholds for pharmacological intervention to prevent fractures. Arch Intern Med. 2004;164(10):1108-12.

31. Wehrli F, Hopkins J, Hwang S, Song H, Snyder P, Haddad J. Cross-sectional study of osteopenia by quantitative magnetic resonance and bone densitometry. Radiology. 2000;217:527-38.

32. Yeung DKW, Griffith JF, Antonio GE, Lee FKH, Woo J, Leung PC. Osteoporosis is associated with increased marrow fat content and decreased marrow fat unsaturation: A proton MR spectroscopy study. J Magn Reson Imaging. 2005;22(2):279-85.

33. Griffith JF, Yeung DK, Antonio GE, Wong SY, Kwok TC, Woo J, et al. Vertebral marrow fat content and diffusion and perfusion indexes in women with varying bone density: MR evaluation. Radiology. 2006;241(3):831-8.

34. Li X, Kuo D, Schafer AL, Porzig A, Link TM, Black D, et al. Quantification of vertebral bone marrow fat content using 3 Tesla MR spectroscopy: reproducibility, vertebral variation, and applications in osteoporosis. J Magn Reson Imaging. 2011;33(4):974-9.

35. Biver E, Durosier-Izart C, Chevalley T, van Rietbergen B, Ri zzoli R, Ferrari S. Evaluation of radius microstructure and areal bone mineral density improves fracture prediction in postmenopausal women. J Bone Miner Res. 2018;33(2):328-37.

36. Seeman E. Growth and age-related abnormalities in cortical structure and fracture risk. Endocrinol Metab (Seoul). 2015;30(4):419-28.

37. Andreasen CM, Delaisse JM, Cj van der Eerden B, van Leeuwen JP, Ding M, Andersen TL. Understanding Age-Induced Cortical Porosity in Women: The

Accumulation and Coalescence of Eroded Cavities Upon Existing Intracortical Canals Is the Main Contributor. J Bone Miner Res. 2018;33(4):606-20.

38.   Syed FA, Oursler MJ, Hefferanm T, Peterson JM, Riggs BL, Khosla S. Effects of estrogen therapy on bone marrow adipocytes in postmenopausal osteoporotic women. Osteoporos Int. 2008;19(9):1323-30.

39.   Rantalainen T, Nikander R, Heinonen A, Cervinka T, Sievänen H, Daly RM. Differential effects of exercise on tibial shaft marrow density in young female athletes. J Clin Endocrinol Metab. 2013;98(5):2037-44.

40.   Belavy DL, Quittner MJ, Ridgers ND, Shiekh A, Rantalainen T, Trudel G. Specific Modulation of Vertebral Marrow Adiposity Tissue by Physical Activity. J Bone Miner Res. 2018;33(4):651-7.

41.   Bolotin H, Sievänen H. Inaccuracies Inherent in Dual-Energy X-Ray Absorptiometry In Vivo Bone Mineral Density Can Seriously Mislead Diagnostic/Prognostic Interpretations of Patient-Specific Bone Fragility. J Bone Miner Res. 2001;16(5):799-805.

42.   Bolotin H, Sievänen H, Grashuis J. Patient-specific DXA bone mineral density inaccuracies: quantitative effects of nonuniform extraosseous fat distributions. J Bone Miner Res. 2003;18(6):1020-7.

Figures

Fig. 1. Co-registration between histologic examination *versus* HR-pQCT imaging;

and marrow fat after Hematoxylin and Eosin (H&E) staining.

Panel A. Scout view of a sheep radius and an example of region of interest (ROI) placement. The first slice of the HR-pQCT image corresponds to the histological cross section. *Panel B.* Half of the cross-section after decalcification and H&E staining. The compact-cortex and the marrow cavity are visible. A distinct adjacent ulna (smaller bone) is also visible. *Panel C*. A magnified view of an area within the marrow cavity shows adipose tissue cells, which appear as empty spaces. This is due to the extraction of fat during processing. *Panel D*. A further magnification of the same area shows adipose tissue more clearly. A cross-section of a trabecula with osteocytes lacunae are also discernible.
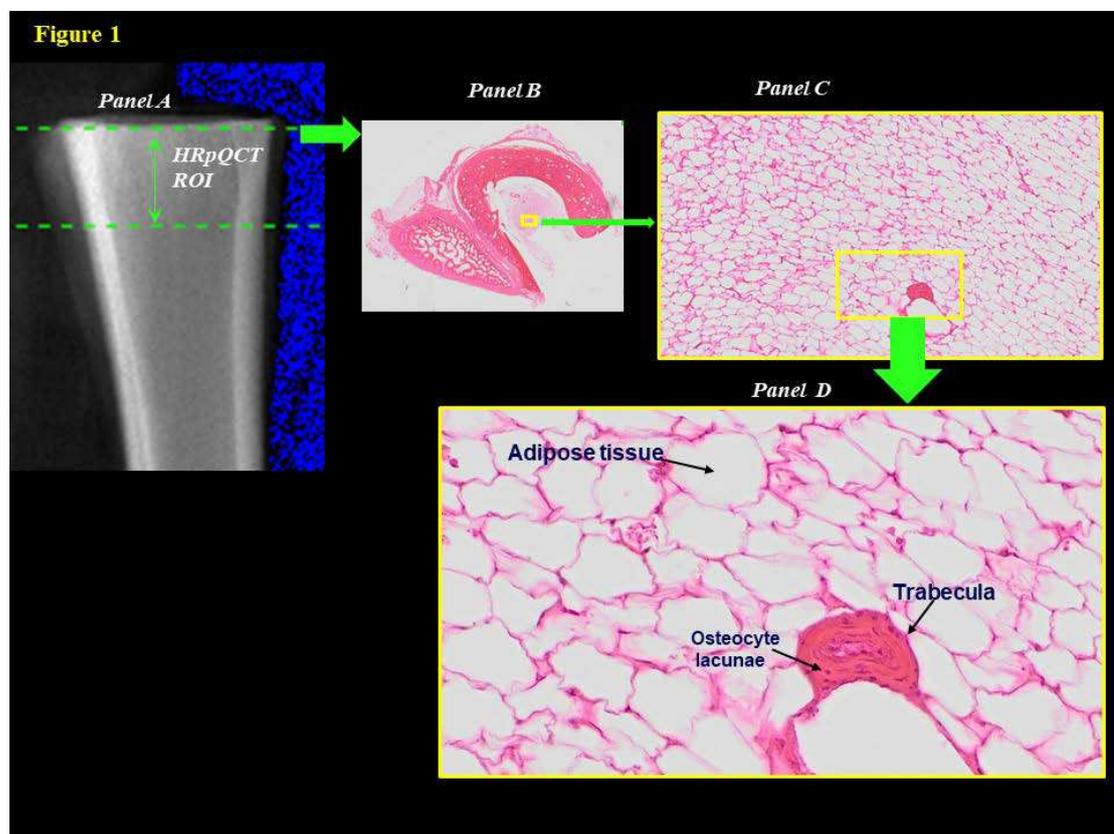
Fig. 2. Participants in the case-control study in 2008-2012.
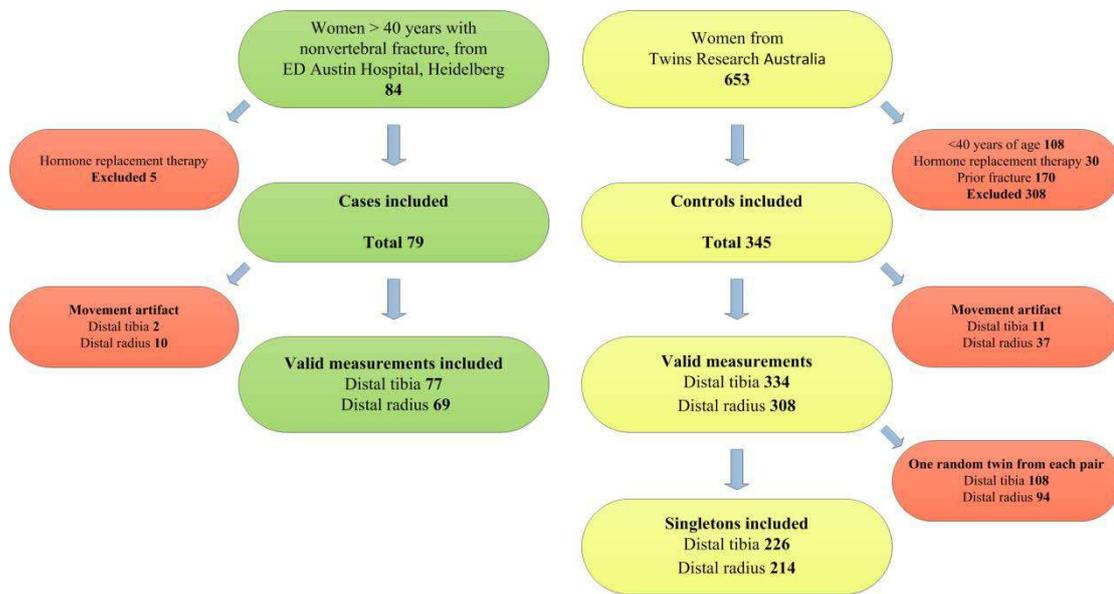
Fig. 3. HR-pQCT image of a human distal radius showing voxels in the marrow cavity that are color-coded in a scale ranging from red to yellow depending on their attenuation relative to water. The larger the proportion of yellow bone marrow (fat cells) than red bone marrow (hematopoietic cells), the lower is the density.

3D display of the medullary cavity at distal radius   Yellow – Red bone marrow
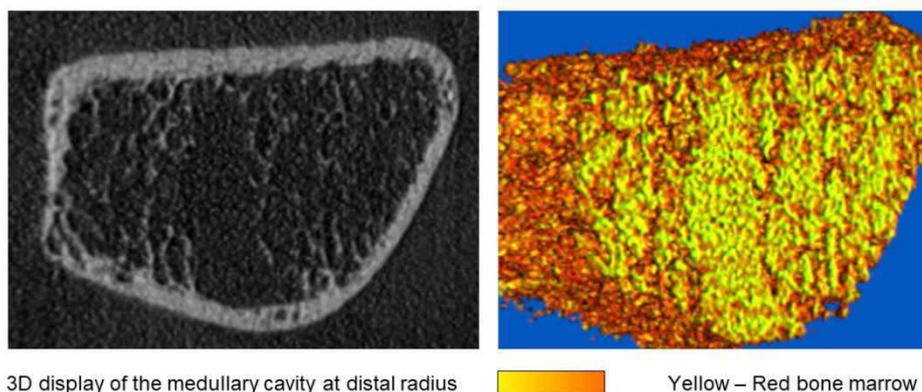
Fig. 4. *Left panel* Correlation of adipose volume (AV) to total marrow volume (TV) (expressed as a percentage) as measured using HR-pQCT *versus* histology (gold standard). *Right panel* shows the corresponding Bland-Altman Plot.

Fig. 4

Accuracy of measurement of adipose volume (AV) to total marrow volume (TV) (%)
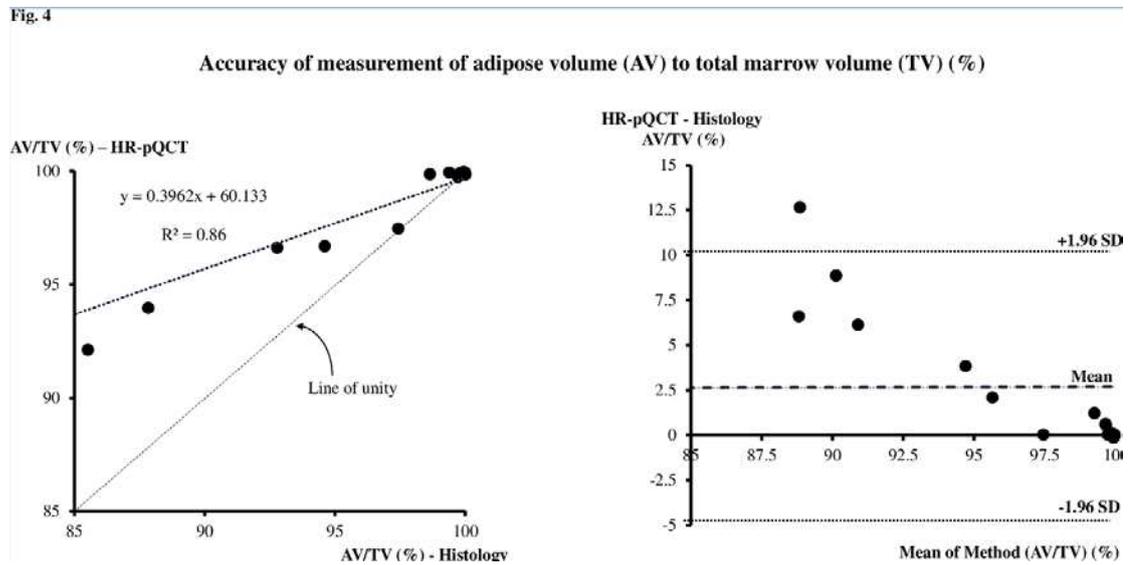
Table 1. Characteristics of women by fracture status

	Cases	Controls	
	n = 77	n = 226	p
Age (years)	54.3 ± 6.4	51.0 ± 8.7	0.002
Height (cm)	162.7 ± 6.5	162.9 ± 6.4	0.818
Weight (kg)	72.3 ± 14.2	70.8 ± 15.5	0.432
Light physical activity (hours/week)	5.0 ± 4.5	4.9 ± 3.5	0.863
Moderate physical activity (hours/week)	1.5 ± 3.3	1.1 ± 2.0	0.091
Vigorous physical activity (hours/week)	0.8 ± 2.2	0.8 ± 1.6	0.109
Physical activity index	10.1 ± 11.1	9.5 ± 7.4	0.551
Premenopausal women, n (%)	11 (14.3)	156 (57.5)	< 0.001
Perimenopausal women, n (%)	10 (13.0)	21 (9.3)	0.355
Postmenopausal women, n (%)	56 (72.7)	75 (33.3)	< 0.001
Femoral neck (FN) aBMD (mg/cm^2)	0.89 ± 0.12	0.98 ± 0.15	< 0.001

FN normal aBMD, n (%)	44 (57.9)	175 (78.5)	< 0.001
FN osteopenia, n (%)	31 (40.8)	44 (19.7)	< 0.001
FN osteoporosis, n (%)	1 (1.3)	4 (1.8)	0.780
Distal Tibia	n = 77	n = 226	
Total cortical porosity (%)	64.5 ± 5.8	60.0 ± 6.2	7.7×10^{-7}
Compact cortex porosity (%)	46.7 ± 7.4	42.1 ± 7.2	0.0001
Outer transitional zone porosity (%)	47.5 ± 6.6	43.1 ± 6.2	1.4×10^{-6}
Inner transitional zone porosity (%)	87.1 ± 3.2	84.7 ± 3.2	9.7×10^{-6}
Cortical thickness (mm)	2.36 ± 0.31	2.34 ± 0.24	0.157
Trabecular number (1/mm)	2.15 ± 0.51	2.76 ± 0.66	3.3×10^{-11}
Trabecular thickness (mm)	0.20 ± 0.01	0.19 ± 0.01	1.1×10^{-5}
Trabecular separation (mm)	1.58 ± 0.31	1.32 ± 0.29	3.2×10^{-8}
Trabecular bone volume/tissue volume (%)	2.93 ± 1.46	4.13 ± 1.73	2.2×10^{-6}
Trabecular volumetric BMD (mg HA/cm³)	111 ± 40.5	131 ± 41.1	0.003
Marrow adiposity index	43.5 ± 3.2	39.9 ± 3.9	5.5×10^{-12}
Distal Radius	n = 69	n = 214	
Total cortical porosity (%)	57.8 ± 5.3	53.7 ± 6.1	1.7×10^{-6}
Compact cortex porosity (%)	40.4 ± 5.3	36.5 ± 5.6	1.2×10^{-6}
Outer transitional zone porosity (%)	43.6 ± 4.9	40.0 ± 4.9	3.7×10^{-8}
Inner transitional zone porosity (%)	86.9 ± 2.7	84.5 ± 2.9	3.1×10^{-6}
Cortical thickness (mm)	1.82 ± 0.19	1.81 ± 0.20	0.870
Trabecular number (1/mm)	1.88 ± 0.55	2.34 ± 0.51	3.0×10^{-8}
Trabecular thickness (mm)	0.20 ± 0.01	0.19 ± 0.01	3.2×10^{-5}
Trabecular separation (mm)	1.65 ± 0.36	1.36 ± 0.30	6.2×10^{-7}
Trabecular bone volume/tissue volume (%)	1.84 ± 1.14	3.04 ± 1.57	3.6×10^{-6}

	98.3 ± 41.5	122 ± 43.0	
Trabecular volumetric BMD (mg HA/cm³)	98.3 ± 41.5	122 ± 43.0	0.009
Marrow adiposity index	48.3 ± 3.4	44.0 ± 4.3	2.4×10^{-11}

Numbers are mean ± standard deviation, or number (%). aBMD = areal bone mineral density.

Cases and controls were compared using semi-parametric regression, adjusted for menopausal status and physical activity as parametric components and age as a non-parametric component.

Table 2. Association of a 1 SD increment in marrow adiposity index (predictor) with each cortical and trabecular trait of distal tibia and distal radius (outcomes)

Outcome variables	Distal tibia			R²	Distal radius			R²
	Coefficient	SE	p		Coefficient	SE	p	
Total cortical porosity (%)	0.334	0.042	2.9×10^{-14}	0.32	0.340	0.050	9.6×10^{-11}	0.29
Compact cortex porosity (%)	0.136	0.043	0.002	0.20	0.168	0.050	0.001	0.19
Outer transitional zone porosity (%)	0.170	0.042	6.8×10^{-5}	0.19	0.205	0.045	8.0×10^{-6}	0.20
Inner transitional zone porosity (%)	0.797	0.035	8.1×10^{-68}	0.66	0.772	0.034	7.8×10^{-65}	0.64
Cortical thickness (mm)	-0.161	0.064	0.012	0.05	-0.058	0.061	0.348	0.003
Trabecular number (1/mm) - linear	-0.601	0.041	9.7×10^{-38}	0.59	-0.700	0.040	6.5×10^{-47}	0.53

	Coefficient	SE	p	R^2	Coefficient	SE	p	R^2
Trabecular thickness (mm)	-0.244	0.062	9.4×10^{-5}	0.10	0.284	0.058	1.6×10^{-6}	0.13
Trabecular separation (mm) - linear	0.723	0.039	3.9×10^{-51}	0.64	0.782	0.035	2.2×10^{-64}	0.64
Trabecular BV/TV (%) - linear	-3.023	0.310	1.2×10^{-19}	0.86	-3.395	0.291	6.1×10^{-26}	0.89
- quadratic	2.084	0.312	1.2×10^{-10}		2.464	0.293	2.1×10^{-15}	
Trabecular vBMD (mg HA/cm³) - linear	-2.542	0.521	1.7×10^{-6}	0.61	-2.886	0.521	7.0×10^{-8}	0.64
- quadratic	1.770	0.522	0.001		2.084	0.525	9.2×10^{-5}	

Coefficient = standardised regression coefficient; SE = standard error; R^2 = Adjusted coefficient of determination (R-square). Semi-parametric regression model was fitted to the data, adjusted for height, weight, physical activity and fracture status whenever significant as parametric components and age as non-parametric component.

Table 3. Fracture risk by 1 standard deviation (SD) increment in cortical and trabecular bone morphology of distal tibia and distal radius

	Odds Ratio (95% CI)	p
Unadjusted analysis		
Age (years) - linear	3.03 (1.88-4.87)	7.1×10^{-6}
- quadratic	0.99 (0.986-0.995)	1.7×10^{-5}
Height (cm)	1.00 (0.96-1.04)	0.830
Weight (kg)	1.01 (0.99-1.02)	0.427
Physical activity (hours/week)	1.01 (0.98-1.04)	0.550
Femoral neck (FN) aBMD (mg/cm^2)	0.52 (0.38-0.70)	2.4×10^{-5}
Distal tibia		
Adjusted for age (quadratic) and FN aBMD		
Total cortical porosity (%)	2.31 (1.53-3.49)	8.7×10^{-5}
Compact cortex porosity (%)	1.90 (1.28-2.81)	0.002
Outer transitional zone porosity (%)	2.22 (1.46-3.36)	2.1×10^{-4}
Inner transitional zone porosity (%)	2.05 (1.34-3.14)	0.001
Cortical thickness (mm)	1.37 (1.03-1.83)	0.033
Trabecular number (1/mm)	0.29 (0.19-0.46)	1.5×10^{-7}
Trabecular thickness (mm)	2.04 (1.50-2.77)	8.5×10^{-6}
Trabecular separation (mm)	2.35 (1.59-3.47)	2.3×10^{-5}
Trabecular bone volume/tissue volume (%)	0.41 (0.26-0.64)	1.4×10^{-4}
Trabecular volumetric BMD (mg HA/cm³)	0.76 (0.53-1.11)	0.158
Marrow adiposity index	3.84 (2.44-6.04)	1.5×10^{-8}
Additional analysis adjusted for all covariates in multivariable models*		
Total cortical porosity (%)	2.62 (1.50-4.58)	0.001
Cortical thickness (mm)	1.56 (1.08-2.28)	0.019

Trabecular thickness (mm)	2.30 (1.61-3.29)	9.7×10^{-6}
Marrow adiposity index	3.60 (2.20-5.90)	8.2×10^{-7}

Distal radius

Adjusted for age (quadratic) and FN aBMD

Total cortical porosity (%)	2.12 (1.48-3.05)	6.0×10^{-5}
Compact cortex porosity (%)	2.21 (1.52-3.21)	4.3×10^{-5}
Outer transitional zone porosity (%)	2.53 (1.67-3.84)	1.9×10^{-5}
Inner transitional zone porosity (%)	2.34 (1.54-3.55)	8.1×10^{-5}
Cortical thickness (mm)	1.11 (0.83-1.49)	0.476
Trabecular number (1/mm)	0.37 (0.25-0.57)	6.1×10^{-6}
Trabecular thickness (mm)	1.95 (1.40-2.70)	9.0×10^{-5}
Trabecular separation (mm)	2.21 (1.51-3.23)	6.1×10^{-5}
Trabecular bone volume/tissue volume (%)	0.35 (0.22-0.57)	3.4×10^{-5}
Trabecular volumetric BMD (mg HA/cm³)	0.71 (0.49-1.03)	0.072
Marrow adiposity index	4.35 (2.67-7.10)	1.1×10^{-8}

Additional analysis adjusted for all covariates in multivariable models*

Total cortical porosity (%)	1.53 (0.99-2.37)	0.054
Trabecular thickness (mm)	2.50 (1.71-3.65)	3.6×10^{-6}
Marrow adiposity index	4.25 (2.50-7.22)	1.9×10^{-7}

*The multivariable logistic regression models were adjusted for age, FN aBMD and all significant covariates. Distal tibia and distal radius variables were standardised to have mean = 0 and SD = 1.

Table 4. Area under the receiver operating characteristic curve (AUC) for the reference model and the incremental contribution of cortical and trabecular bone morphology of distal tibia and distal radius to prediction of fracture

	AUC	95% CI	Change in AUC	p
Distal Tibia				
Reference model 1: age, age² and FN aBMD	0.751	0.69-0.81		
Total cortical porosity (%)	0.796	0.74-0.85	**0.045**	**0.006***
Compact cortex porosity (%)	0.778	0.72-0.84	**0.028**	**0.039***
Outer transitional zone porosity (%)	0.794	0.74-0.85	**0.043**	**0.007***
Inner transitional zone porosity (%)	0.776	0.71-0.84	0.025	0.119*
Cortical thickness (mm)	0.758	0.70-0.82	0.007	0.556*
Trabecular number (1/mm)	0.825	0.77-0.88	**0.074**	**0.0002***
Trabecular thickness (mm)	0.790	0.73-0.85	**0.040**	**0.034***
Trabecular separation (mm)	0.798	0.74-0.85	**0.048**	**0.009***
Trabecular bone volume/tissue volume (%)	0.787	0.73-0.85	0.037	0.060*
Trabecular volumetric BMD (mg HA/cm³)	0.755	0.69-0.82	0.004	0.594*
Marrow adiposity index (MAI)	0.825	0.77-0.88	**0.075**	**0.002***
Reference 2: age, age², FN aBMD and MAI			Ref 2	
Total cortical porosity (%)	0.843	0.79-0.89	**0.017**	**0.049****
Trabecular number (1/mm)	0.847	0.80-0.89	**0.022**	**0.023****
Trabecular thickness (mm)	0.870	0.83-0.91	**0.044**	**0.007****
Distal Radius				
Reference model 1: age, age² and FN aBMD	0.742	0.68-0.81		
Total cortical porosity (%)	0.788	0.73-0.85	**0.047**	**0.013***
Compact cortex porosity (%)	0.791	0.73-0.85	**0.050**	**0.010***
Outer transitional zone porosity (%)	0.796	0.73-0.86	**0.054**	**0.007***

Inner transitional zone porosity (%)	0.775	0.71-0.84	0.034	0.116*
Cortical thickness (mm)	0.742	0.68-0.81	0.001	0.889*
Trabecular number (1/mm)	0.772	0.73-0.85	**0.051**	**0.027***
Trabecular thickness (mm)	0.775	0.71-0.84	0.034	0.119*
Trabecular separation (mm)	0.778	0.72-0.84	0.037	0.079*
Trabecular bone volume/tissue volume (%)	0.788	0.73-0.85	0.046	0.051*
Trabecular volumetric BMD (mg HA/cm³)	0.745	0.68-0.81	0.003	0.764*
Marrow adiposity index (MAI)	0.833	0.78-0.89	**0.092**	**0.001***
Reference 2: age, age², FN aBMD and MAI			Ref 2	
Total cortical porosity (%)	0.840	0.79-0.89	0.006	0.311**
Trabecular number (1/mm)	0.835	0.78-0.89	0.001	0.797**
Trabecular thickness (mm)	0.882	0.84-0.93	**0.048**	**0.009***

P-value for difference in AUC when compared to *reference model 1 and **reference model 2.

FN aBMD = femoral neck areal bone mineral density.